A Density Functional Theory Study of the $Cu^+ \cdot O_2$ and $Cu^+ \cdot N_2$ Adducts

Jamal N. Dawoud[a], Ismail I. Fasfous[a], and Amin F. Majdalawieh[b]

[a] Department of Chemistry, Faculty of Science, Hashemite University, Zarqa 13115, P. O. Box 150459, Jordan
[b] Department of Biology, Chemistry and Environmental Sciences, Faculty of Arts and Sciences, American University of Sharjah, Sharjah, P. O. Box 26666, United Arab Emirates

Reprint requests to Jamal N. Dawoud. E-mail: jamaldawoud@hu.edu.jo

Z. Naturforsch. **2012**, *67b,* 118 – 126; received November 16, 2011

The geometries and harmonic vibration frequencies of the $Cu^+ \cdot O_2$ and $Cu^+ \cdot N_2$ are determined by various density functional theory (DFT) methods employing different basis sets. The potential energy surfaces (PES) are examined. The $Cu^+ \cdot O_2$ adduct exhibits a bent structure with a binding energy of 12.4 kcal mol^{-1}, whereas $Cu^+ \cdot N_2$ exhibits a linear configuration with a binding energy of 23.5 kcal mol^{-1}. The binding energy values for the two adducts agree well with the available published experimental and theoretical data and hence are reliable.

Key words: Copper Ion Complexes, Potential Energy Surface, Gas Separation, Binding Energies, NBO Analysis, Oxygen, Nitrogen

Introduction

Separation of oxygen from nitrogen and production of oxygen-enriched air are important industrial processes that have been under extensive examination theoretically and experimentally. For many years, gas separation using different types of adsorbents, such as zeolites, has been the focus of many studies. Special attention was given to adsorbents containing transition metal complexes due to their potential capability to allow separation of oxygen from air [1]. This separation process is based on the extent of the physical adsorption of O_2 and N_2 gases. In addition, it was found that zeolites containing Cu cations show high catalytic activity toward the decomposition of NO into O_2 and N_2 [2]. However, the structure and chemical properties of the Cu sites in various types of zeolites have still not been fully revealed due to experimental obstacles owing to low Cu concentrations in Cu-ZSM-5 [3].

The interaction of N_2 with Cu cations in zeolite has been experimentally studied using IR spectroscopy [2] and guided ion beam mass spectrometry [4]. For the $[Cu{\cdot}N_2]^+$ complex in zeolite, the vibration frequency was found to be 2297 cm^{-1} at r. t. [2]. In addition, the results of DFT analyses of the $[Cu \cdot N_2]^+$ complex were found to be in good agreement with the experimental findings [2, 4, 5]. These theoretical calculations were limited to the global minimum of the complex for which the structure and binding energy were determined [2, 6].

The interaction of the Cu^+ ion with molecular O_2 was examined using the relativistic effective core potential at the level of the CCSD(T) approach [7]. The geometrical parameters as well as the binding energies were calculated for specific orientations of the $Cu^+ \cdot O_2$ complexes at different spin states. Recently, the adsorption process of O_2 over the $Cu^{\delta+}$-montmorillonite cluster [$Cu^{\delta+}$-MMT] was examined, in which the structure and binding energy of O_2 with Cu^+ were obtained using the BLYP/TZP method [8]. The authors concluded that the interaction between O_2 and the active site of $Cu^{\delta+}$-MMT is of physical adsorption type with a binding energy of 13.3 kcal mol^{-1}.

Few studies have been conducted to elucidate the interaction in $Cu^+ \cdot N_2$ and $Cu^+ \cdot O_2$ [5 – 8]. However, the exact physical parameters governing these interactions were not completely elucidated. In this paper, we examine the structure and potential energy surface for the global, local and transition states of $Cu^+ \cdot N_2$ and $Cu^+ \cdot O_2$. The results are discussed and interpreted in the light of the available literature data.

Theoretical Details

The molecular geometry of the $Cu^+ \cdot N_2$ and $Cu^+ \cdot O_2$ adducts were optimized using different DFT methods. In particular, B3LYP, B3P86 and B3PW91

methods have been employed based on the GAUSSIAN 03 suite program [9]. Pseudo potentials of "LANL2DZ and LANL2TZ" basis set function types were employed only for Cu, whereas standard all electron Pople-type 6-31+G(d) and 6-311+G(df) basis sets were utilized for the atoms of the gases O_2 and N_2.

The potential energy surfaces (PES) of the $Cu^+ \cdot N_2$ and $Cu^+ \cdot O_2$ adduct have been obtained using the intrinsic reaction coordinate (IRC) [10, 11]. Vibration frequency tests were used to determine which minimum represents the saddle point and to calculate the zero point energy (ZPE) and its thermodynamic properties at T = 298 K for each stationary point on the curve. For each complex, the binding energy was calculated by subtracting the total energy of the adduct $Cu^+ \cdot X_2$ from the total energy of the un-complexed moieties, Cu^+ and X_2, including the zero point correction. The resulting binding energy was then subjected to the basis set superposition error (BSSE) using the full counterpoise method [12, 13].

For the adduct formation $Cu^+ + X_2 \rightarrow [Cu \cdot X_2]^+$ the thermodynamic parameters were calculated. In particular, ΔH^o was calculated using the following formula [14],

$$\Delta H^o = \sum_{\text{products}} E_{\text{corr}} - \sum_{\text{reactants}} E_{\text{corr}} \qquad (1)$$

where, E_{corr} is the corrected electronic energy including the zero point energy and enthalpy thermal corrections. This term is calculated directly from the frequency test for each stationary point. The same procedure was applied for calculating ΔG^o for the $[Cu \cdot X_2]^+$ adduct interaction.

To get a deeper insight into the electronic structure and bonding properties of $Cu^+ \cdot O_2$ and $Cu^+ \cdot N_2$, the electronic parameters and atomic charges of the two adducts at different structures were calculated according to the natural bond orbital (NBO) analysis procedure [15]. These calculations were performed on the basis of the B3P86/6-311+G(df) wave functions.

Results and Discussion

The $Cu^+ \cdot O_2$ adduct

The intrinsic reaction coordinates of $Cu^+ \cdot O_2$ obtained at the UB3LYP level of theory indicate the existence of one minimum and two transition states. The minimum has a bent structure whereas the two saddle points of first order-type exhibit T-shaped and linear structures as illustrated in Fig. 1.

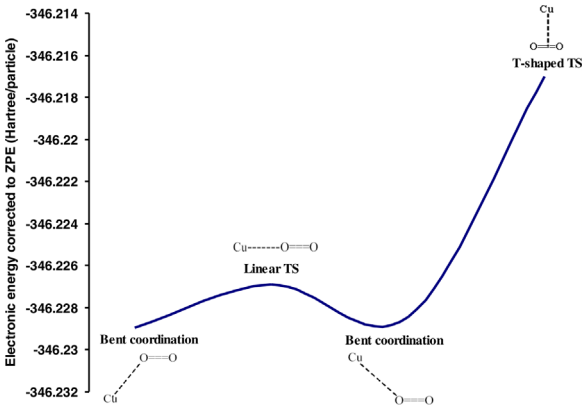

Fig. 1. The potential energy surface of the $Cu^+ \cdot O_2$ adduct calculated at the UB3LYP/LANL2TZ (Cu^+),6-311+G(df)(O_2) level of theory.

The optimized geometry parameters and harmonic vibration frequencies of $Cu^+ \cdot O_2$ at different configurations are given in Tables 1 and 2, respectively. At all levels of DFT, the results of the calculated geometrical parameters are in good agreement. For example, the UB3LYP/LANL2TZ/6-311+G(df) results of the geometrical parameters of the bent coordination are found to be $r_{(Cu\text{-}O)}$ = 2.1 Å, $r_{(O\text{-}O)}$ = 1.21 Å and ∠(Cu–O–O) = 135.7°, which are in good agreement with the CCSD(T)-optimized values of the bond lengths and angles as may be seen from Table 1. In addition, our findings are slightly different from those obtained by Briones-Jurado and Agacino-Valdés [8] (see Table 1). It is noteworthy that their computational results were obtained on the level of the BLYP/TPZ method including the interaction of N_2 and O_2 gases with the Cu^+ ion in the MMT cluster [8].

As shown in Table 1, the O–O bond length in $Cu^+ \cdot O_2$ was found to be slightly longer than that of the free O_2 molecule. Importantly, the highest σ vibration obtained using different DFT methods of 1593 cm^{-1} [calculated on the basis of the UB3LYP/LANL2TZ/6-311+G(df) method] for the bent coordination is in good agreement with the experimental value of 1544.7 cm^{-1} for $\omega(O_2)$ as well as with the calculated value of 1587 cm^{-1} obtained from the DFT method [16]. For the two transition state structures, it was found that the highest harmonic frequency values obtained using the UB3LYP level of theory are slightly smaller than those obtained using the UB3P86 and UB3PW91 levels of theory (see Table 2). However, all DFT meth-

Table 1. Geometrical parameters of the $Cu^+ \cdot O_2$ adduct in different orientations.

Geometry	Method	Basis set	r_1(O–O) (Å)	r_2(Cu–O) (Å)	θ_1 (deg)[a]
Bent coordination	UB3LYP	LANL2DZ/6-31+G(d)	1.218	2.042	129.0
		LANL2DZ/6-311+G(df)	1.206	2.050	137.0
		LANL2TZ/6-31+G(d)	1.219	2.017	127.9
		LANL2TZ/6-311+G(df)	1.207	2.021	135.7
Free O_2		6-311+G(df)	1.199	–	–
	UB3PW91	LANL2DZ/6-31+G(d)	1.211	2.048	129.0
		LANL2DZ/6-311+G(df)	1.201	2.054	137.5
		LANL2TZ/6-31+G(d)	1.211	2.023	128.3
		LANL2DZ/6-311+G(df)	1.201	2.024	135.8
Free O_2		6-311+G(df)	1.198	–	–
	UB3P86	LANL2DZ/6-31+G(d)	1.211	2.022	128.5
		LANL2DZ/6-311+G(df)	1.201	2.028	136.9
		LANL2TZ/6-31+G(d)	1.211	1.998	127.8
		LANL2TZ/6-311+G(df)	1.202	2.001	135.6
Free O_2		6-311+G(df)	1.198	–	–
Bent coordination[b]	CCSD(T)	BS1	1.286	2.168	166.1
Bent coordination[c]	UBLYP	TZP	1.249	1.866	118.4
T-shaped TS	UB3LYP	LANL2DZ/6-31+G(d)	1.231	2.277	74.3
		LANL2DZ/6-311+G(df)	1.219	2.338	74.9
		LANL2TZ/6-31+G(d)	1.234	2.224	73.9
		LANL2TZ/6-311+G(df)	1.222	2.286	74.5
	UB3PW91	LANL2DZ/6-31+G(d)	1.223	2.289	74.5
		LANL2DZ/6-311+G(df)	1.211	2.355	75.1
		LANL2TZ/6-31+G(d)	1.226	2.230	74.0
		LANL2DZ/6-311+G(df)	1.214	2.298	74.7
	UB3P86	LANL2DZ/6-31+G(d)	1.224	2.238	74.1
		LANL2DZ/6-311+G(df)	1.212	2.303	74.8
		LANL2TZ/6-31+G(d)	1.228	2.185	73.7
		LANL2TZ/6-311+G(df)	1.215	2.250	74.3
T-shaped[c]	CCSD(T)	BS1	1.310	2.535	75.0
Linear TS	UB3LYP	LANL2DZ/6-31+G(d)	1.213	2.036	180.0
		LANL2DZ/6-311+G(df)	1.204	2.026	180.0
		LANL2TZ/6-31+G(d)	1.213	2.016	180.0
		LANL2TZ/6-311+G(df)	1.204	2.012	180.0
	UB3PW91	LANL2DZ/6-31+G(d)	1.206	2.044	180.0
		LANL2DZ/6-311+G(df)	1.201	2.031	180.0
		LANL2TZ/6-31+G(d)	1.206	2.022	180.0
		LANL2TZ/6-311+G(df)	1.202	2.013	180.0
	UB3P86	LANL2DZ/6-31+G(d)	1.206	2.019	180.0
		LANL2DZ/6-311+G(df)	1.201	2.007	180.0
		LANL2TZ/6-31+G(d)	1.206	2.011	180.0
		LANL2TZ/6-311+G(df)	1.201	2.004	180.0
Linear[c]	CCSD(T)	BS1	1.280	2.137	180.0

[a] ∠Cu–O1–O2 bond angle; [b] taken from ref. [7]; [c] taken from ref. [8].

ods applied here yielded reasonable harmonic frequencies that compared well with the experimental findings.

The NBO population analysis of the $Cu^+ \cdot O_2$ complex in different configurations was performed using the common UB3P86/6-311+G(df){O_2}/LANL2DZ{Cu} calculations. The NBO analysis of the atomic charges listed in Fig. 2 showed that the electronic charge of the Cu^+ ion in the bent coordination is not significantly changed, whereas the first oxygen atom (O1) directly attached to the Cu^+ ion gains electronic charge from the second oxygen atom (O2). The charge redistribution of the O_2 moiety in the complex is due to the polarization of the π electrons of molecular O_2. This indicates that the copper ionic charge causes a strong electric field on O_2 suggesting that pure electrostatic interactions are dominant, mainly, charge-quadrupole and charge-induced dipole interactions. In addition, a very small variation in the metal ionic charge indicates a weak interaction between the HOMO (π^*_{2p} orbital) of the O_2 moiety and the LUMO (4*s* orbital) of the Cu^+ ion since the

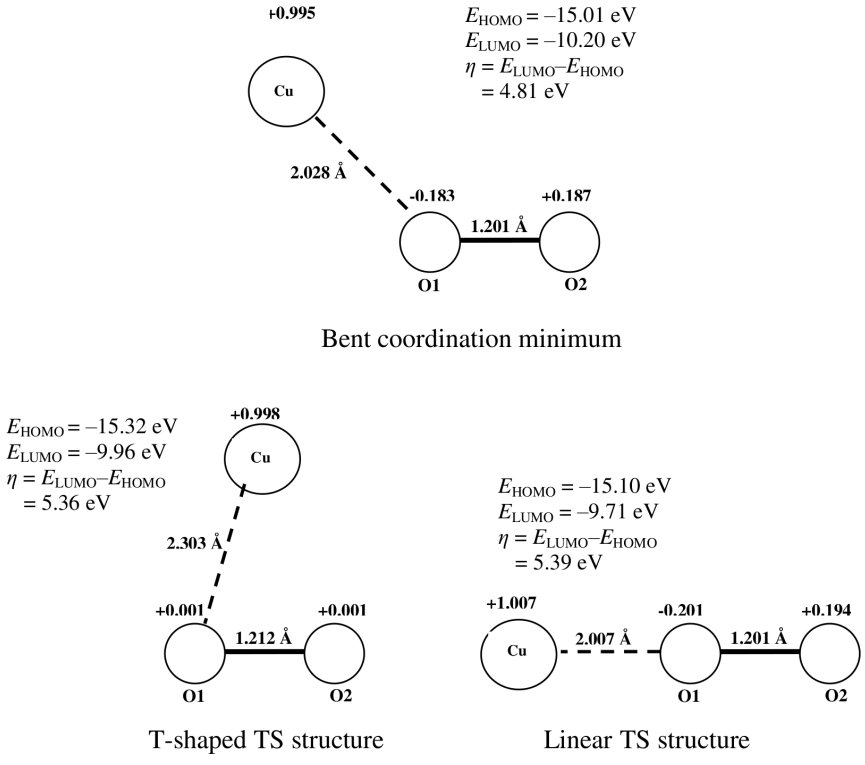

Fig. 2. NBO atomic charges of each atom in the $Cu^+ \cdot O_2$ adduct at different states calculated on the basis of the UB3P86/LANL2DZ(Cu^+), 6-311+G(df)(O_2) level of theory.

Table 2. Harmonic vibrational frequencies of the $Cu^+ \cdot O_2$ adduct calculated with different DFT methods using the LANL2TZ (Cu^+)/6-311+G(df) (O_2) basis set.

Method	Vibrational frequencies (cm^{-1})
Bent coordination minimum	
UB3LYP	134.0(σ), 262.4(π), 1528(σ)
UB3P86	137.2(σ), 265.7(π), 1637.5(σ)
UB3PW91	134.2(σ), 252.6(π), 1638.0(σ)
T-shaped transition state	
UB3LYP	153.6(a_1), 249.2i(b_2), 1533.5(a_1)
UB3P86	157.7(a_1), 249.9i(b_2), 1570.8(a_1)
UB3PW91	147.5(a_1), 244.4i(b_2), 1580.8(a_1)
Linear transition state	
UB3LYP	247.2(a_1), 111.8i(b_2), 1636.7(a_1)
UB3P86	248.6(a_1), 110.5i(b_2), 1679.5(a_1)
UB3PW91	238.5(a_1), 108.6i(b_2), 1678.0(a_1)

value of $HOMO(O_2 - \pi^*_{2p}) \leftrightarrow LUMO(Cu^+_{4s})$ energy gap (4.81 eV) is relatively large.

For the T-shaped transition state, the atomic charge distribution shows that the Cu^+ ion as well as the O_2 moiety keep most of their charges. This means that the interaction between them is of repulsive nature, which pushes the Cu^+ ion away from the O_2 moiety to a distance of 2.29 Å, which is larger than the displacement distance observed for the bent coordination (2.02 Å). The second transition state with a linear structure has a charge distribution that is similar to that obtained for the global minimum (see Fig. 2). Note here that according to the NBO analysis the variation in the charge of the Cu^+ ion in three structures is very small. This indicates that the $HOMO(O_2 - \pi^*_{2p}) \leftrightarrow LUMO(Cu^+_{4s})$ interaction may have little influence on the interaction between the Cu^+ ion and the O_2 moiety in the complex.

Electronic and bonding properties in the $Cu^+ \cdot O_2$ adduct

The NBO population analysis of the corresponding orbitals between the metal ion and the O_2 moiety, in different configurations, were calculated and compared with those of its components. For the minimum and transition state structures, the natural charge of the copper ion as well as the 3*d*, 4*s* and 4*p* orbital populations were calculated and listed in Table 3. The Cu^+ ion in its ground state is a d^{10} closed-shell system, while in the adducts with bent, T-shaped and linear structures the population of the 4*s* orbital is not negligible, indicating that the valence electrons of the copper ion are redistributed with a sizable charge transfer from an O_2 lone pair to the metal ion except for the latter struc-

	Cu^+	O_2	$Cu^+ \cdot O_2$ (bent coordination)	$Cu^+ \cdot O_2$ (T-shaped TS)	$Cu^+ \cdot O_2$ (linear TS)
q_{Cu}	+1.000	–	+0.995	+0.998	+1.007
3*d*	10.000	–	9.948	9.966	9.955
4*s*	0.000	–	0.052	0.033	0.033
4*p*	0.000	–	0.005	0.007	0.006
(2s,2p$_{x,y,z}$) O1	–	5.966	6.146 (▲ 0.180)	5.967(▲ 0.001)	6.168(▲ 0.202)
(2s,2p$_{x,y,z}$) O2	–	5.966	5.781 (▼ 0.185)	5.967(▲ 0.001)	5.774(▼ 0.192)

Table 3. Natural atomic charges, 3*d*, 4*s* and 4*p* populations of the Cu^+ ion and total population of the valence shell of each oxygen atom in the O_2 molecule in different structures performed at the UB3P86/LANL2DZ(Cu^+), 6-311+G(df)(O_2) level of theory[a].

[a] ▲: amount of increase relative to free O_2, ▼: amount of decrease relative to free O_2.

Geometry	Method	Basis set	BE	$\Delta H^0_{298\,K}$	$\Delta G^0_{298\,K}$	BSSE
Bent coordination	UB3LYP	LANL2TZ/6-311+G(df)	12.4	−12.9	−7.4	1.70
	UB3PW91	LANL2TZ/6-311+G(df)	12.7	−13.1	−7.7	0.15
	UB3P86	LANL2TZ/6-311+G(df)	12.7	−13.1	−7.6	1.63
Bent coordination[a]	CCSD(T)	BS1	12.3	–	–	–
T-shaped TS	UB3LYP	LANL2TZ/6-311+G(df)	4.9	−5.7	0.13	1.42
	UB3PW91	LANL2TZ/6-311+G(df)	5.3	−6.1	−0.6	0.36
	UB3P86	LANL2TZ/6-311+G(df)	6.3	−7.1	−1.8	0.32
T-shaped[a]	CCSD(T)	BS1	5.4	–	–	–
Linear TS	UB3LYP	LANL2TZ/6-311+G(df)	11.2	−12.1	−3.2	1.93
	UB3PW91	LANL2TZ/6-311+G(df)	10.0	−10.9	−2.0	1.90
	UB3P86	LANL2TZ/6-311+G(df)	11.5	−12.3	−3.4	1.88
Linear[a]	CCSD(T)	BS1	11.8	–	–	–

Table 4. Binding energy (BE), thermodynamic data, $\Delta H^0_{298\,K}$ and $\Delta G^0_{298\,K}$, and BSSE, for the $Cu^+ \cdot O_2$ adduct, at the level of various theories. The units are in kcal mol^{-1}.

[a] Taken from ref. [7].

ture. In all structures, an electronic charge transfers from 3*d* orbitals toward the 4*s* orbital occurs, the population thus increasing by 0.052, 0.032 and 0.033 for the bent, T-shaped and linear structures, respectively. This indicates some 3*d*-4*s* mixing (hybridization) and hence reduction in the metal-O_2 repulsion enhancing the binding interaction. A similar behavior is observed for the O_2 moiety in the complex (see Table 3). For the bent structure, it was found that the total population of the valence orbitals of molecular O_2 is slightly reduced as a result of a weak σ donation. Consequently, the interaction process is largely of an electrostatic type. A similar behavior is also observed in the T-shaped transition state structure.

Table 3 indicates that for the complex in its linear structure a small amount of electrons is transferred from the 3*d* orbitals of the Cu^+ ion and distributed mainly on the 4*s* and 4*p* orbitals of the Cu^+ ion whereas the remaining electrons transfer to the LUMO of the O_2 moiety. This is consistent with the slight increase in the positive charge located on the copper ion (see Fig. 2).

Binding energies of the $Cu^+ \cdot O_2$ adduct

The binding and associated basis set superposition energies of the $Cu^+ \cdot O_2$ adduct in different configurations were calculated by various DFT methods (UB3LYP, UB3P86 and UB3PW91) (see Table 4). In all cases, the computed values of the binding energies are consistent and reliable. Notably, our best value for the binding energy of the $Cu^+ \cdot O_2$ adduct, in the bent structure, is 12.4 kcal mol^{-1}, which is highly consistent with the values of 12.3 and 13.3 kcal mol^{-1} that obtained theoretically at the CCSD(T)/BS1 [7] and BLYP/TZP [8] levels of theory, respectively. Furthermore, our best value, that was calculated at the UB3LYP/LANL2TZ/6-311+G(df) level of theory, is in good agreement with 11.0 kcal mol^{-1} that inferred from experiments [17].

Our best values of the computed binding energies [11.5 kcal mol^{-1} for the linear and 5.3 kcal mol^{-1} for the T-shaped structure (see Table 4)] agree very well with the values of 11.8 and 5.4 kcal mol^{-1} calculated at the level of the CCSD(T) method [7], respectively. As expected, the binding energy of the linear transition state structure was found to be close to the global minimum binding energy. Since there are no experimental and theoretical thermodynamic data, the $\Delta H^{O}_{298\,K}$ and $\Delta G^{O}_{298\,K}$ values for the $Cu^+ \cdot O_2$ complex in its global minimum structure were calculated to be −13.0 and −7.6 kcal mol^{-1}, respectively.

The $Cu^+ \cdot N_2$ adduct

The results of the geometry optimizations and harmonic frequency calculations for the $Cu^+ \cdot N_2$ adduct ($^1\Sigma^+$ state) are given in Tables 5 and 6, respectively. According to the IRC diagram presented in Fig. 3, we considered both the linear and the T-shaped structures.

Table 5. Geometrical parameters of the $Cu^+ \cdot N_2$ adduct in different orientations.

Geometry	Method	Basis set	r_1(N–N) (Å)	r_2(Cu–N) (Å)	θ_1 (deg)[a]
Linear coordination	B3LYP	LANL2DZ/6-31+G(d)	1.105	1.967	180.0
		LANL2DZ/6-311+G(df)	1.094	1.951	180.0
		LANL2TZ/6-31+G(d)	1.105	1.941	180.0
		LANL2TZ/6-311+G(df)	1.093	1.927	180.0
Linear coordination[b]	B3LYP	ECP/TZVP	1.093	1.923	180.0
Free N_2		6-311+G(df)	1.093	–	–
	B3PW91	LANL2DZ/6-31+G(d)	1.101	1.939	180.0
		LANL2DZ/6-311+G(df)	1.093	1.939	180.0
		LANL2TZ/6-31+G(d)	1.104	1.932	180.0
		LANL2DZ/6-311+G(df)	1.093	1.915	180.0
Free N_2		6-311+G(df)	1.093	–	–
	B3P86	LANL2DZ/6-31+G(d)	1.104	1.944	180.0
		LANL2DZ/6-311+G(df)	1.093	1.925	180.0
		LANL2TZ/6-31+G(d)	1.104	1.918	180.0
		LANL2TZ/6-311+G(df)	1.092	1.902	180.0
Free N_2		6-31+G(df)	1.092	–	–
T-shaped TS	B3LYP	LANL2DZ/6-31+G(d)	1.112	2.291	76.0
		LANL2DZ/6-311+G(df)	1.101	2.315	76.1
		LANL2TZ/6-31+G(d)	1.113	2.259	75.8
		LANL2TZ/6-311+G(df)	1.101	2.280	76.0
	B3PW91	LANL2DZ/6-31+G(d)	1.108	2.283	75.9
		LANL2DZ/6-311+G(df)	1.101	2.304	76.2
		LANL2TZ/6-31+G(d)	1.113	2.248	75.4
		LANL2DZ/6-311+G(df)	1.101	2.265	75.9
	B3P86	LANL2DZ/6-31+G(d)	1.112	2.253	75.7
		LANL2DZ/6-311+G(df)	1.101	2.272	76.0
		LANL2TZ/6-31+G(d)	1.113	2.222	75.5
		LANL2TZ/6-311+G(df)	1.101	2.238	75.8

[a] ∠Cu–N1–N2 bond angle; [b] taken from ref. [6].

Table 6. Harmonic vibration frequencies of the $Cu^+ \cdot N_2$ adduct calculated by different methods of DFT using LANL2TZ (Cu^+)/6-311+G(df) (N_2) basis set.

Method	Vibration frequencies (cm^{-1})
Linear coordination minimum	
B3LYP	313.1(σ), 245.1(π), 2450.3(σ)
B3P86	321.1(σ), 250.8(π), 2462.9(σ)
B3PW91	312.2(σ), 250.0(π), 2458.6(σ)
T- shaped transition state	
B3LYP	194.6(a_1), 227.3i(b_2), 2367.0(a_1)
B3P86	206.6(a_1), 219.7i(b_2), 2374.7(a_1)
B3PW91	194.4(a_1), 218.2i(b_2), 2376.1(a_1)

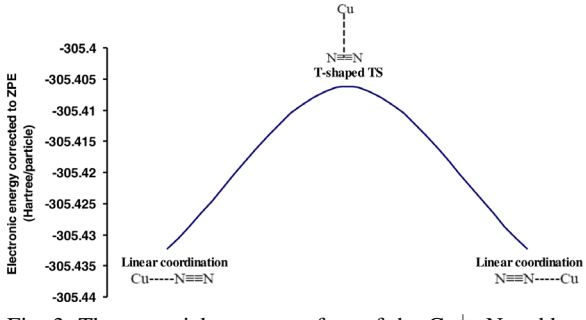

Fig. 3. The potential energy surface of the $Cu^+ \cdot N_2$ adduct calculated at the B3LYP/LANL2TZ(Cu^+),6-311+G(df)(N_2) level of theory.

We found that the T-shaped structure was a saddle point, obtained from internal rotation of N_2, and being the saddle point between the two equivalent linear structures. The agreement between the different levels of DFT theory is again very good. Delabie *et al.* [6] optimized the geometry of $Cu^+ \cdot N_2$ in its linear structure at the B3LYP/ECP{Cu}/TZVP{N_2} level of theory, where $r_{(Cu\text{-}N)}$ was calculated to be 1.923 Å – reasonably close to our best value of 1.927 Å calculated at the B3LYP/LANL2TZ/6-311+G(df) level of theory. In addition, the $r_{(N\text{-}N)}$ value of 1.093 Å agrees well with the experiment (1.098 Å) obtained for the free N_2 molecule using rotational Raman spectroscopy [18] as well as with the theoretical value of 1.093 Å [6]. The same result is obtained for the T-shaped structure, where a reasonable agreement is found among the calculated geometrical parameters using various DFT methods.

The harmonic vibration frequencies were calculated by various DFT methods. Our best value of the N–N stretching frequency (2450.3 cm^{-1}) calculated on the basis of the B3LYP/LANL2TZ/6-311+G(df) level of theory, agrees well with the values previously obtained (at DFT: 2333 cm^{-1} [2] and at LSDA: 2387 cm^{-1}) [5].

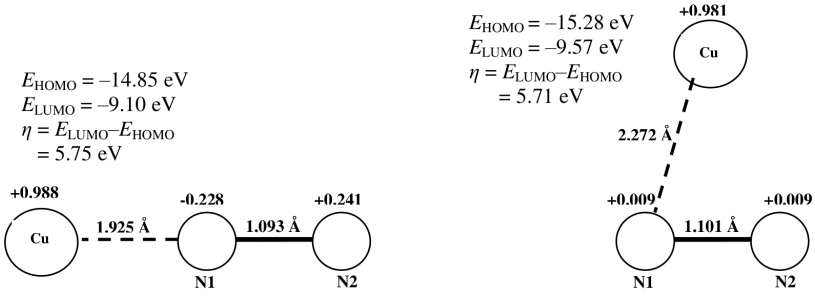

Linear structure minimum T-shaped TS structure

Fig. 4. NBO atomic charges of each atom in the $Cu^+ \cdot N_2$ adduct at different states calculated on the basis of the B3P86/LANL2DZ(Cu), 6-311+G(df)(N_2) level of theory.

For the T-shaped transition state structure, the N–N stretching frequency is closer to the experimental and theoretical values of the free N_2 molecule [18, 19] (see Table 6).

The NBO population analysis of the atomic charges of the $Cu^+ \cdot N_2$ adduct indicates that the interaction between the Cu^+ ion and the N_2 moiety in its linear structure is stronger than that in the T-shaped structure as illustrated in Fig. 4. It was found that the charge distribution of the N_2 molecule in the adduct is highly polarized, since the nitrogen atom directly attached to the Cu^+ ion exhibits a partial charge of -0.23, whereas the second nitrogen atom has a charge of $+0.24$ (Fig. 4). This is due to the π electrons largely migrating toward the nitrogen atom nearest to the Cu^+ ion as a result of high attraction forces between them.

The atomic charge distribution of the T-shaped structure, presented in Fig. 4, indicates that the interaction between the Cu^+ ion and the N_2 moiety is of repulsive nature. This may reduce the stability of the T-shaped structure, and hence, push the Cu^+ ion away from the N_2 molecule to further distance as compared with the linear configuration (see Table 5).

Electronic and bonding properties in the $Cu^+ \cdot N_2$ adduct

The atomic population of the corresponding orbitals in $Cu^+ \cdot N_2$ in different structures were calculated and compared with those of the Cu^+ ion and the N_2 molecule before complexation. These results are summarized in Table 7. In all structures, the electron density of the 3*d* orbitals of the Cu^+ ion was reorganized, and an electronic charge transfer from the 3*d* orbitals [$3d^{10} \rightarrow 3d^{9.921}$ (linear) and $3d^{9.960}$ (T-shaped TS)] toward the 4*s* orbital the population of which increases by 0.090 and 0.053 for the linear and T-shaped structures, respectively, took places. Furthermore, a similar behavior is observed for the N_2 moiety in the adduct, where the electron density of the valence shell is slightly redistributed. It appears that the π electrons mainly migrated toward the nitrogen atom directly attached to the Cu^+ ion. The population of the 3*d* orbitals in the two structures of $Cu^+ \cdot N_2$ is lower than 10 indicating a sizable electron transfer mainly to the 4*s* orbital. Such electron delocalization process indicates that the Cu–N linkage has a dative bond character. Table 7 shows that an electronic charge transfer from the HOMO (σ_{2p}) of O_2 to the LUMO (4*s*) of the Cu^+ ion is favorable but still relatively weak since the bond length of the N_2 molecule is not significantly changed.

Table 7. Natural charges, 3*d*, 4*s* and 4*p* populations of the Cu^+ ion and total population of the valence shell of each nitrogen atom in the N_2 molecule in different structures performed at the B3P86/LANL2DZ(Cu^+), 6-311+G(df)(N_2) level of theory[a].

	Cu^+	N_2	$Cu^+ \cdot N_2$ (linear coordination minimum)	$Cu^+ \cdot N_2$ (T-shaped TS)
q_{Cu}	+1.000	–	+0.988	+0.981
3*d*	10.000	–	9.921	9.960
4*s*	0.000	–	0.090	0.053
4*p*	0.000	–	0.001	0.002
(2s,2p$_{x,y,z}$) N1	–	4.952	5.178 (▲ 0.226)	4.944(▼ 0.008)
(2s,2p$_{x,y,z}$) N2	–	4.952	4.715 (▼ 0.237)	4.944(▼ 0.008)

[a] ▲: amount of increase relative to free N_2, ▼: amount of decrease relative to free N_2.

It is worthwhile to mention that the quadrupole moment of the N_2 molecule (-1.463 D Å) is 3.5 times larger than that of the O_2 molecule (-0.403 D Å) [19], and hence, the electrostatic interaction within the $Cu^+ \cdot N_2$ adduct is expected to be larger than that of the $Cu^+ \cdot O_2$ complex. In addition, the Cu^+ ion is found to be closer to the N_2 moiety in the $Cu^+ \cdot N_2$ adduct, compared to distance of the O_2 moiety in $Cu^+ \cdot O_2$. Consequently, the binding energy of the $Cu^+ \cdot N_2$ adduct is

Geometry	Method	Basis set	BE	$\Delta H^0_{298\,K}$	$\Delta G^0_{298\,K}$	BSSE
Linear coordination	B3LYP	LANL2TZ/6-311+G(df)	22.5	−23.1	−16.2	2.33
	B3PW91	LANL2TZ/6-311+G(df)	21.7	−22.4	−15.4	2.23
	B3P86	LANL2TZ/6-311+G(df)	23.5	−24.2	−17.2	2.21
Linear coordination[a]	CCSD(T)	Large ANO	22.9	–	–	–
Linear coordination[b]	Expt.	–	21.2 ± 7	–	–	–
T-shaped TS	B3LYP	LANL2TZ/6-311+G(df)	6.9	−7.7	−1.8	1.56
	B3PW91	LANL2TZ/6-311+G(df)	6.2	−7.0	−1.2	1.52
	B3P86	LANL2TZ/6-311+G(df)	7.6	−8.5	−2.6	1.54

Table 8. Binding energy (BE), thermodynamic data, $\Delta H^0_{298\,K}$ and $\Delta G^0_{298\,K}$, and BSSE, for the $Cu^+ \cdot N_2$ addulct at the level of various DFT methods. The units are in kcal mol^{-1}.

[a] Taken from ref. [6]; [b] taken from ref. [4].

expected to be larger than that of the $Cu^+ \cdot O_2$ adduct as presented in the next section.

The difference in the geometry of the global minima of the two adduct (bent "$Cu^+ \cdot O_2$" *vs.* linear "$Cu^+ \cdot N_2$") may be explained by two factors. In particular, the bonding modes exhibited by N_2 and O_2 are slightly different. This is reflected in the interaction process within the adduct. For example, the total population of atomic valence orbitals indicates that the electrons involved in the Cu^+–O_2 interaction are the lone pairs of the O_2 molecule [the s, p_z orbitals largely reorganize in the complex with respect to the isolated O_2 molecule (results not shown)]. In addition, the angle between the Cu^+ ion and the O_2 molecule in the bent coordination ($\theta \cong 130.0^\circ$) suggests sp^2 hybridization for the O_2 molecule in the complex. For $Cu^+ \cdot N_2$ in its linear configuration the population of the atomic valence orbitals ($2s$ and $2p$ orbitals) is also redistributed as a result of polarization (result not shown). Furthermore, the attraction forces between the Cu^+ ion and the lone pairs (sp hybridization) induce a linear coordination ($\theta = 180.0^\circ$). The second factor is the difference in the strength of the electrostatic interaction between the metal ion and the O_2 and N_2 species. The $Cu^+ \cdot N_2$ adduct exhibits a stronger electrostatic interaction. Consequently, the Cu^+–N bond length is shorter than the Cu^+–O bond length by a value of 0.1 Å (see Tables 1 and 4).

Binding energies of the $Cu^+ \cdot N_2$ adduct

The binding energies of $Cu^+ \cdot N_2$ in the linear and T-shaped structures were calculated by various DFT methods, with the results given in Table 8. In all cases, the results obtained by these methods are relatively consistent and reliable. We found that the linear structure exhibits the strongest binding energy between the Cu^+ ion and the N_2 moiety with a binding energy of 22.5 kcal mol^{-1} (B3LYP/LANL2TZ/6-311+G(df)). Our best value agrees very well with the values of 22.9 and 23.2 kcal mol^{-1} obtained by the CCSD(T) [6] and BP86 methods [5], respectively. Furthermore, our DFT results of the binding energy of the linear $Cu^+ \cdot N_2$ structure agree very well with the experimental value of 21.2 ± 7 kcal mol^{-1} [4] (see Table 8). For the saddle point, the T-shaped structure exhibits a larger repulsive interaction that reduces its binding energy to a value of 6.8 kcal mol^{-1}.

Unfortunately, experimental and theoretical results of the thermodynamic data for the $Cu^+ \cdot N_2$ adduct are lacking, but one could at least propose that the negative sign of $\Delta H^0_{298\,K}$ indicates that the formation of this adduct in its linear structure is exothermic (see Table 8).

Conclusions

The equilibrium geometries and harmonic vibration frequencies of $Cu^+ \cdot O_2$ and $Cu^+ \cdot N_2$ have been calculated by various DFT methods. They show convergence with the basis set that was used. $Cu^+ \cdot O_2$ exhibits a bent equilibrium geometry, with a Cu^+–O bond length of 2.03 Å, an O–O bond length of 1.21 Å and a $\angle$(Cu–O–O) bond angle of 132°. The binding energy of $Cu^+ \cdot O_2$ was calculated to be 12.4 kcal mol^{-1}, which agrees well with the available theoretical and experimental results. On the other hand, $Cu^+ \cdot N_2$ exhibits a linear equilibrium geometry, with a Cu^+–N bond length of 1.93 Å and an N–N bond length of 1.096 Å. The binding energy of $Cu^+ \cdot N_2$ was calculated to be 22.5 kcal mol^{-1}, which agrees very well with the theoretical findings on the CCSD(T) level of theory as well as with experimental findings. The binding energies and geometrical parameters calculated using different DFT methods agree well with CCSD(T) and experimental data (where available) in the case of the $Cu^+ \cdot N_2$ adduct.

Electrostatic interaction appears to be the predominant driving force in $Cu^+ \cdot N_2$ as may be seen from the high polarization of the π electrons of the N_2 moiety, which creates a stronger interaction with the Cu^+ ion (see Fig. 4). This feature has less effect in the $Cu^+ \cdot O_2$

adduct due to the small quadrupole moment of the O_2 moiety. In addition the hybridization of the valence orbitals of the two species $\{(N_2\ (sp),\ O_2\ (sp^2)\}$ plays an important role in the interaction process within the adduct.

Acknowledgement

J. N. D would like to thank the Deanship of Research and Graduate Studies at the Hashemite University (Jordan) for the financial support of this work.

[1] H. Kawakami, H. Iwanaga, M. Iwamoto, S. Kagawa, *J. Chem. Soc., Chem. Commun.* **1982**, 1396.
[2] E. Broclawik, J. Datka, B. Gil, W. Piskorz, P. Kozyra, *Topics in Catal.* **2000**, *11/12*, 335.
[3] W. F. Schneider, K. C. Hass, R. Ramprasad, J. B. Adams, *J. Phys. Chem.* **1996**, *100*, 6032.
[4] M. T. Rodgers, B. Walker, P. B. Armentroat, *Int. J. Mass Spectrom.* **1999**, *182/183*, 99.
[5] W. F. Schneider, K. C. Hass, R. Ramprasad, J. B. Adams, *J. Phys. Chem. B* **1998**, *102*, 3692.
[6] A. Delabie, K. Pierloot, *J. Phys. Chem. A* **2002**, *106*, 5679.
[7] J. Hrušák, W. Koch, H. Schwarz, *J. Chem. Phys.* **1994**, *101*, 3898.
[8] C. Briones-Jurado, E. Agacino-Valdés, *Int. J. Quant. Chem.* **2008**, *108*, 1802.
[9] M. J. Frisch, G. W. Trucks, H. B. Schlegel, G. E. Scuseria, M. A. Robb, J. R. Cheeseman, J. A. Montgomery, Jr., T. Vreven, K. N. Kudin, J. C. Burant, J. M. Millam, S. S. Iyengar, J. Tomasi, V. Barone, B. Mennucci, M. Cossi, G. Scalmani, N. Rega, G. A. Petersson, H. Nakatsuji, M. Hada, M. Ehara, K. Toyota, R. Fukuda, J. Hasegawa, M. Ishida, T. Nakajima, Y. Honda, O. Kitao, H. Nakai, M. Klene, X. Li, J. E. Knox, H. P. Hratchian, J. B. Cross, C. Adamo, J. Jaramillo, R. Gomperts, R. E. Stratmann, O. Yazyev, A. J. Austin, R. Cammi, C. Pomelli, J. W. Ochterski, P. Y. Ayala, K. Morokuma, G. A. Voth, P. Salvador, J. J. Dannenberg, V. G. Zakrzewski, S. Dapprich, A. D. Daniels, M. C. Strain, O. Farkas, D. K. Malick, A. D. Rabuck, K. Raghavachari, J. B. Foresman, J. V. Ortiz, Q. Cui, A. G. Baboul, S. Clifford, J. Cioslowski, B. B. Stefanov, G. Liu, A. Liashenko, P. Piskorz, I. Komaromi, R. L. Martin, D. J. Fox, T. Keith, M. A. Al-Laham, C. Y. Peng, A. Nanayakkara, M. Challacombe, P. M. W. Gill, B. Johnson, W. Chen, M. W. Wong, C. Gonzalez, J. A. Pople, GAUSSIAN 03 (revision B.05), Gaussian, Inc., Pittsburgh PA (USA) **2003**.
[10] C. Gonzalez, H. B. Schlegel, *J. Chem. Phys.* **1989**, *90*, 2154.
[11] C. Gonzalez, H. B. Schlegel, *J. Phys. Chem.* **1990**, *94*, 5523.
[12] F. E. Budenholzer, E. A. Gislason, A. D. Jorgensen, *Chem. Phys.* **1986**, *110*, 171.
[13] S. Ikuta, *Chem. Phys. Lett.* **1984**, *109*, 550.
[14] M. I. Alomari, J. N. Dawoud, *J. Mol. Struct. (Theochem)* **2010**, *939*, 28.
[15] O. S. Sizova, *J. Mol. Struct. (Theochem)* **2006**, *760*, 183.
[16] G. V. Chertihin, L. Andrews, C. W. Bauschlicher, Jr., *J. Phys. Chem. A* **1997**, *101*, 4026.
[17] J. Valyon, W. K. Hall, *J. Catal.* **1993**, *143*, 520.
[18] L. C. Hoskins, *J. Chem. Educ.* **1975**, *52*, 568.
[19] D. B. Lawson, J. F. Harrison, *J. Phys. Chem. A* **1997**, *101*, 4781.